Gait Phase Estimation Based on Noncontact Capacitive Sensing and Adaptive Oscillators

Enhao Zheng, Silvia Manca, Tingfang Yan, Andrea Parri, Nicola Vitiello, *Member, IEEE*, and Qining Wang*, *Member, IEEE*

***Abstract*—This paper presents a novel strategy aiming to acquire an accurate and walking-speed-adaptive estimation of the gait phase through noncontact capacitive sensing and adaptive oscillators (AOs). The capacitive sensing system is designed with two sensing cuffs that can measure the leg muscle shape changes during walking. The system can be dressed above the clothes and free human skin from contacting to electrodes. In order to track the capacitance signals, the gait phase estimator is designed based on the AO dynamic system due to its ability of synchronizing with quasi-periodic signals. After the implementation of the whole system, we first evaluated the offline estimation performance by experiments with 12 healthy subjects walking on a treadmill with changing speeds. The strategy achieved an accurate and consistent gait phase estimation with only one channel of capacitance signal. The average root-mean-square errors in one stride were 0.19 rad (3.0% of one gait cycle) for constant walking speeds and 0.31 rad (4.9% of one gait cycle) for speed transitions even after the subjects rewore the sensing cuffs. We then validated our strategy in a real-time gait phase estimation task with three subjects walking with changing speeds. Our study indicates that the strategy based on capacitive sensing and AOs is a promising alternative for the control of exoskeleton/orthosis.**

***Index Terms*—Gait phase estimation, orthosis, exoskeleton, capacitive sensing, adaptive oscillators.**

I. Introduction

RECENT developments in lower-limb exoskeletons/orthoses extend the mobility of people with gait impairments and reduce the payload of the nursing staff [1], [2]. They can not only assist people's locomotion in daily activities [3]–[9], but also improve the recovery efficacy in pathological gait rehabilitation [10], [11]. In order to accomplish different tasks, various types of mechanical structures (from the previous rigid ones [1] to the emerging soft "exosuits" [9], [12], [13]) and control approaches (e.g. pre-recorded gait trajectory control [3], [4], model-based control [5], [6], the fuzzy-classifiers-based control [7] and the adaptive-oscillators-based (AOs-based) control [14], [15]) have been designed and developed. However, challenges still exist in developing safe and seamless human-robot interaction in locomotion tasks of daily use.

One of the main issues in this field is to accurately infer the user's gait phase information, which is also the primary step to control the lower-limb exoskeletons/orthosis [16]. To achieve this goal, researchers designed sensing systems and algorithms to firstly record human motion information and then translate the raw signals to specific gait phases [17]. Among the signals that can be measured by current wearable sensing technologies, inertial signals (Euler angles, acceleration, angular velocity, etc.) [6], [9], [18]–[23] and foot pressure signals (ground reaction force or foot switches) [4], [5], [8], [24]–[26] are more widely used. The foot pressure signals can be measured by foot insoles or switches. The signals directly convey gait information with physical significance. The inertial signals can be measured by inertial measurement units (IMUs). Compared with foot pressure sensors, the IMUs can record stable and repeatable gait information during the swing period. In addition to these two sensing approaches, there are some researchers using surface electromyography (sEMG) signals [27], [28] for gait estimation. The post-processing algorithms include the discrete gait phase detection [5], [9], [18], [21], [25], [27] and the continuous gait phase estimation [29]–[31]. The discrete gait phase detection methods segment the gait cycle into several discrete sub-phases with the designed models, such as hidden Markov model [21], fuzzy logic [25], machine learning [18], etc. The

Manuscript received August 15, 2016; revised December 11, 2016; accepted February 11, 2017. Date of publication February 23, 2017; date of current version September 18, 2017. This work was supported in part by the Beijing Disabled Persons' Federation, in part by the National Natural Science Foundation of China under Grant 91648207, in part by the Beijing Municipal Science and Technology Project (Z151100000915073), in part by the Beijing Nova Program (Z141101001814001), in part by the EU within the CYBERLEGs project (FP7-ICT-2011-2.1) under the Grant Agreement 287894, and in part by Fondazione Pisa within the IUVO project (prog. 154/11). *Asterisk indicates corresponding author. (Nicola Vitiello and Qining Wang contributed equally to this paper.)*.

E. Zheng was with the Robotics Research Group, College of Engineering, Peking University. He is now with the State Key Laboratory of Management and Control for Complex Systems, Institute of Automation, Chinese Academy of Sciences.

S. Manca and A. Parri are with The BioRobotics Institute, Scuola Superiore Sant'Anna, Pisa, Italy.

T. Yan was with The BioRobotics Institute, Scuola Superiore Sant'Anna, Pisa, Italy. She is now with The Chinese University of Hong Kong.

N. Vitiello is with The BioRobotics Institute, Scuola Superiore Sant'Anna, Pisa, Italy, and also with Fondazione Don Carlo Gnocchi, Firenze, Italy.

*Q. Wang is with the Robotics Research Group, College of Engineering and the Beijing Innovation Center for Engineering Science and Advanced Technology, Peking University, Beijing 100871, China (e-mail: qiningwang@pku.edu.cn).

This paper has supplementary downloadable material available at http://ieeexplore.ieee.org, provided by the authors. The material includes a video, titled CSensAOs.avi, showing the real-time gait phase estimation based on the proposed noncontact capacitive sensing and adaptive oscillators (File size: 68 MB).

Digital Object Identifier 10.1109/TBME.2017.2672720

continuous gait phase estimation is achieved by estimating the percentage of one gait cycle either by historical stride durations [29] or by a pool of adaptive oscillators [30], [31].

Although great efforts have been made by previous studies, limitations still exist. Firstly, for inertial sensors (mainly IMUs), drifts can affect the consistency of the signals. In order to compensate the drifts, additional computations and more sensors have to be used which increases the complexity of the whole system [17]. Another limitation of IMUs is that the rigid sensor nodes on human body can influence the human motion and the performance of the system is also affected by the vigorous motions [32]. Secondly, for the foot pressure sensors, the lifespan of the pressure sensors—often made of load cells and force sensitive resistors (FSRs)—were limited due to the repetitive load [33]. The limited life span reduces the reliability of the system in long time use. For the exoskeletons without ankle joint, additional sensor-embedded devices (insoles [26] or foot switches [8]) have to be dressed on feet and fabricated based on the feet sizes, which increases inconvenience and obtrusiveness. Additionally, for sEMG sensors, the electrodes have to be firmly in contact with human skin. The performance is affected by motion artifacts, sweating and sensing spots.

In order to compensate these limitations, we provide another solution based on noncontact capacitive sensing and the AOs-based estimator. The noncontact capacitive sensing method was previously proposed to recognize amputees' locomotion modes [34], [35]. Compared with sEMG based method, the strategy produced equally well recognition results and it overcame the drawbacks of sEMG sensors by freeing human skin from contacting to electrodes. The AOs dynamic system was previously applied in lower-limb exoskeletons/orthoses [14], [31], [36]. Thanks to the inherent synchronization properties of the AOs, the AOs dynamic system showed great merits in walking speed adaptation and continuous phase estimation. It also extend the ability of providing a continuous finely-tuned assistance to exoskeleton control [31].

The objective of this study is to provide a gait phase estimation strategy which is able to: i) reliably estimate the gait phase from the information of the leg, which makes the apparatus be easily integrated with exoskeletons and overcomes the drawbacks of the existing sensing approaches; ii) produce accurate and continuous gait phase estimation when there are walking speed changes and when the sensing device is re-worn. The contributions of this study are listed as follows. Firstly, we proposed a gait phase estimation strategy based on noncontact capacitive sensing and an AOs-based estimator. The noncontact capacitive sensing system was designed to record leg muscle deformations during level ground walking with two cuffs, one on the thigh and the other on the shank. The AOs-based estimator was coupled with the capacitance signals and continuously estimated the gait phase at different walking speeds. Secondly, the stability and adaptivity of the phase estimation system was offline evaluated with data collected during treadmill walking at different speeds. The performance of the system was also evaluated when it was exposed to disturbance brought by re-wearing the sensing device, which was a relevant issue for wearable sensing devices and orthosis in practical use. Thirdly, the effectiveness of the whole strategy was validated in a real-time estimation with subjects walking on the treadmill at different speeds.

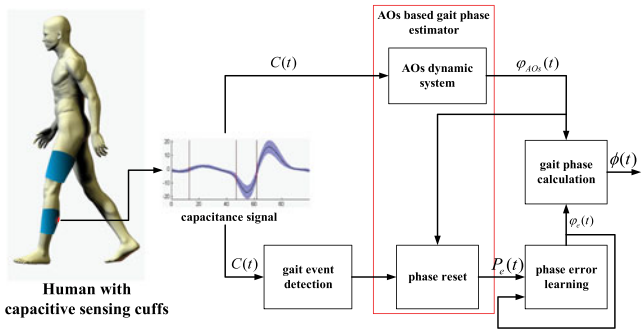

Fig. 1. Structure of the gait phase estimation strategy based on noncontact capacitive sensing and the adaptive oscillators. $C(t)$ stands for the capacitance signal recorded from the capacitive sensing system. $\varphi_{\mathrm{AOs}}(t)$ stands for the phase initially learned by adaptive oscillator algorithm. $P_e(t)$ stands for the phase reset error. $\varphi_e(t)$ stands for the phase error learned from the reset error learning procedure. $\phi(t)$ stands for the final output of the gait phase estimator.

II. Estimation Strategy

In this study, the gait phase was continuously estimated through the capacitive sensing system and an adaptive gait phase estimator (as shown in Fig. 1). Our designed sensing system measured leg muscle deformations by two cuffs (on the thigh and the shank, respectively). The selected capacitance signal ($C(t)$, usually one channel of the signals) was input to the AOs-based gait phase estimator to provide continuous phase estimation. The gait phase estimation algorithm comprised the AOs dynamic system, the gait event detection block, the phase reset block, the phase error learning block and the gait phase calculation block. The AOs dynamic system firstly estimated the gait phase $\varphi_{\mathrm{AOs}}(t)$ by tracking the periodic capacitance signals with several oscillators. The phase reset block then calculated the phase reset error $P_e(t)$ at the time of gait event detected by the gait event detection block. The phase error learning block acquired a smooth estimation of the phase error $P_e(t)$, which was then used to correct the initial phase variable $\varphi_{\mathrm{AOs}}(t)$. Finally, the gait phase calculation block output the accurate and continuous gait phase $\phi(t)$.

A. Capacitive Sensing System

The designed capacitive sensing system was composed of two sensing cuffs and the signal processing circuits. The sensing cuffs encircled the thigh and the shank, respectively. Six capacitive electrodes were fixed on the inner surface of each sensing cuff. For each sensing cuff, three electrodes were distributed in the anterior part and the other three on the posterior part. A layer of silicon rubber was placed (2.5-mm thickness) on the electrodes to isolate them from conductors. The sensing principle of the capacitive sensing in this study was shown in Fig. 2. The human body and the capacitive electrodes were conductors. They were separated by the silicon rubbers and cloth (in the middle of the two conductors). Therefore, each electrode

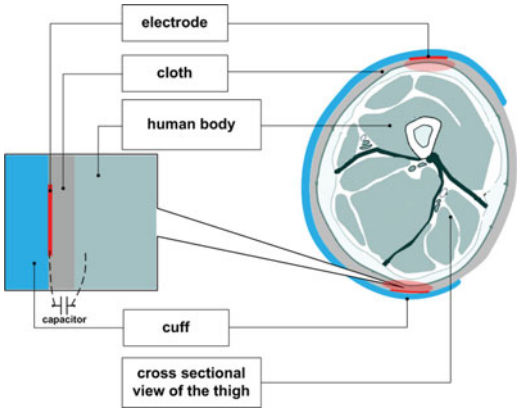

Fig. 2. The sensing principle of the noncontact capacitance sensing system. The right part of the figure shows the cross section of the human leg with the sensing cuff. The capacitance electrodes are adhered to the inner surface of the sensing cuff. The electrodes and human body form the equivalent capacitor as is shown in the left part.

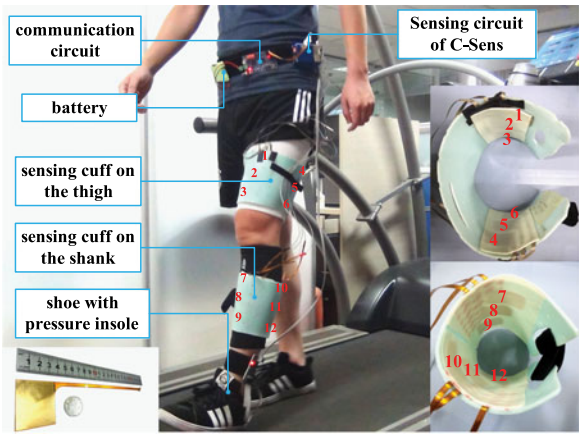

Fig. 3. Placement of the capacitive sensing system on human body while walking on the treadmill. The foot pressure insole is placed inside the shoe. All the sensing circuits are fixed on the waist with bandage. The top right of the figure shows the thigh cuff, while the bottom right shows the shank cuff. The electrodes are covered with a layer of silicon film with thickness of 2 mm. The red numbers denote the channel number of the sensing system of that position. The left bottom of the figure shows one electrode of the capacitive sensing system. The electrode is fabricated with Flex-PCB, and the surface is made of copper. It has a thickness of 0.2 mm.

with human body made constituted a plate capacitors. During locomotion, the leg muscle deformations change the distance between the human body and the electrodes. As a results, the capacitance signal changes periodically. The gait phase information can be obtained by recording the capacitance signals.

The electrodes of the sensing system (right part of Fig. 3) were made of flexible printed circuit boards (Flex-PCB). The sensing cuffs were made of thermoplastic materials which could be easily shaped when heated up to 70 °C. The cuffs were shaped according to the leg profile of the user. We also mounted a bandage on the medial side of the cuff to secure it tight on the leg (right bottom of Fig. 3). The signal processing circuits included a sensing circuit and a communication circuit. The sensing circuit sampled capacitance signals by measuring the charging-and-recharging cycle time of the capacitors. A reference capacitor on the circuit mapped the charging time to actual capacitance values. The sensing circuit could sample capacitance values from 12.5 pF to 800 pF with 18-bit (approximate) digital resolution and with a sampling frequency of 100 Hz. The signal ground of the sensing circuit was connected to human body via an electrode arbitrarily placed inside the sock. The communication circuit was used to synchronize the capacitive sensor data with other sensors and to transmit the data to the computer.

B. Adaptive-Oscillator-Based Gait Phase Estimator

The gait phase estimator consisted of three subsystems, namely an AOs-based dynamic system, a gait event detector and a phase error compensator. The AOs dynamic system was aimed to primarily acquire a continuous phase variable $\varphi_{\mathrm{AOs}}(t)$ by tracking the different harmonics of the periodic capacitance signals [14], [31], [36]. The phase reset block calculated the phase reset error $P_e(t)$ at the time of gait event detected. Finally, the phase error learning block acquired a continuous estimation of the phase error $P_e(t)$ which was then used to correct the initial phase variable $\varphi_{\mathrm{AOs}}(t)$, and output the accurate and continuous gait phase $\phi(t)$.

1) AO Dynamic System: The key part of the gait phase estimator (see Fig. 1) is the AOs dynamic system. Adaptive oscillators can learn and synchronize with the cyclical signals adaptively and quickly [14], [15]. This dynamics of AOs provides an opportunity to extract the fundamental features of the periodic signal, such as the phase, frequency, amplitude and offset. The features are learned and stored in the dedicated state variables of the AOs. The state variables are updated on each sample based on the errors between the input signals and the reconstructed signals. The AOs actually decompose the input signal into its frequency components with each oscillator learning one harmonic. The phase and the frequency of each harmonic wave are extracted to estimate the phase of the cyclical monitored task. According to [31], [36], the state space equations of the AOs are expressed as follows:

$$\dot{\varphi}_k = \omega(t) \cdot i + \nu_\varphi \frac{F(t)}{\Sigma\alpha_k} \cos(\varphi_k(t)) \tag{1}$$

$$\dot{\omega}(t) = \nu_\omega \frac{F(t)}{\Sigma\alpha_k} \cos(\varphi_1(t)) \tag{2}$$

$$\dot{\alpha}_k(t) = \eta F(t) \sin(\varphi_k(t)) \tag{3}$$

$$\dot{\alpha}_0(t) = \eta F(t) \tag{4}$$

where ω is the fundamental harmonic frequency; φ_k and α_k are the phase and the amplitude of the k-th oscillator, respectively, capturing the contribution of the k-th harmonic; α_0 is the offset component of the input. $F(t) = \theta(t) - \hat{\theta}(t)$, which is the difference between the periodic input signal $\theta(t)$ and the corresponding estimated one $\hat{\theta}$(t) actuates the evolution of each state variable along time t. The learning speeds for phase, fre-

quency and amplitude are determined by constant gains ν_φ, ν_ω and η. The parameters were selected by analyzing the features (amplitude and offsets) of the capacitance signals following our previous experience [31] and initial off-line attempts. The real-time estimate of the input signal is computed as a sum of each oscillator, limited to N harmonics (the number of N in this study was 3):

$$\hat{\theta}(t) = \sum_{k=1}^{N} \alpha_k(t) \sin(\varphi_k(t)) + \alpha_0(t) \tag{5}$$

2) Event Detection Block: This block (Fig. 1) implements the detection of a desired event in one stride that it is used to identify the starting of a new gait cycle. The zero phase value of the gait phase from AOs should be matched with this event. The characteristic event can be either a physically significant event of the stride (for instance, the heel strike) or a periodical feature of the input signal (for instance, its maximum peak). In our study, as the capacitance signals were quasi-sinusoidal within one stride, we used the positive maximum peak of the capacitance signal from the selected channels as the desired gait event.

3) Phase Reset and Phase Error Learning: The estimated gait phase $\phi(t)$ is a variable continuously changing from 0 to 2π rad within one stride. It is computed within the gait phase calculation block (Fig. 1) that combines the information output by the phase error learning block and the AOs dynamical system block. The time-normalized variable is linearly correlated with the percentage of one gait cycle with 0 rad matching the detected gait event. The initial estimation of gait phase $\varphi_{\mathrm{AOs}}(t)$ is obtained by normalizing the phase of fundamental harmonic component into [0, 2π). In order to match the estimated 0 rad with the detected gait event, the phase reset error learning block computes the mismatch $P_e(t_k)$ between the 0-rad related event and the actual phase estimate provided by the AOs:

$$P_e(t_k) = \begin{cases} -\varphi_{\mathrm{AOs}}(t_k), & 0 \le \varphi_{\mathrm{AOs}}(t_k) < \pi \\ 2\pi - \varphi_{\mathrm{AOs}}(t_k), & \pi \le \varphi_{\mathrm{AOs}}(t_k) < 2\pi. \end{cases} \tag{6}$$

The phase reset block resets the phase to 2π when the C-Sens signal reached its maximum peak. The phase error reset value $P_e(t_k)$ is the difference between the estimated phase and the ideal phase (0 rad) in correspondence of the relevant biomechanical event. To smoothly compensate the phase error, a state variable $\varphi_e(t)$ is introduced to learn $P_e(t_k)$ within one stride cycle. The learning rule is expressed as:

$$\dot{\varphi}_e = \epsilon(t_k)\omega(t)e^{-\omega(t)(t-t_k)} \tag{7}$$

where, $\epsilon(t_k) = \kappa_p[P_e(t_k) - \varphi_e(t_k)]$ is an error determining the desired variation of $\varphi_e(t)$ during one stride cycle; κ_p is a proportional gain; $\omega(t)$ is the signal frequency tracked by AOs dynamic system. The equation is is a first-order system filtering a fraction of the phase error at event detection and is used to guarantee stability and convergence of the phase error learning system. After this learning procedure, continuous estimated gait phase can be obtained by:

$$\phi(t) = \mathrm{mod}(\varphi_{\mathrm{AOs}}(t) + \varphi_e(t), 2\pi) \tag{8}$$

III. Experimental Validation

A. Experimental Protocol

We carried out two experiments to evaluate our gait phase estimation strategy. The first experiment (Exp1) was to evaluate the performance of the strategy with changing walking speeds and with re-wearing the sensing devices. In Exp1, twelve male able-bodied subjects (25.7 ± 4.2 years old, 71.6 ± 7.4 kg weight and 176.4 ± 4.7 cm height) were recruited. All subjects provided written and informed consent. The experiment was also approved by the Local Ethics Committee of Peking University (Beijing, China). The sensing cuffs were dressed on the left leg. For the shank, we placed the cuff above the Gastrocnemius which is the most prominent part to prevent the cuff from slipping. The other sensing cuff was placed above the knee at the middle portion of the thigh. One foot pressure insole was placed in the shoe of the measured leg to detect the critical gait events for initial analysis. Four FSRs (FlexiForce A401, Tekscan, Inc., MA, USA) were placed on the insole to sample the vertical ground reaction force (GRF). Before the experiment of each subject, we measured the signals of foot pressure insole when the measured leg rested freely above the ground for 10 seconds and stood still for 10 seconds. We summed the data of four positions and averaged the data over 10 seconds of the two measurements. The initial measurement procedure was used for computing the threshold to segment the gait cycle. The placement of the whole system on human body was shown in Fig. 3. All sensor data were synchronized by the communication circuit which transmitted the sensor data to a computer via Bluetooth. The data sampling rate was 100 Hz. The pressure insoles were fabricated based on subjects' feet sizes and were placed inside their left shoes. The signal processing circuits and a Lion battery (8.4V) were fixed on the waist by velcro bandages (Fig. 3). There were two sessions (Session I and Session II) of measurement in Exp1. In each session, the subjects were asked to walk on the treadmill with three different speeds, i.e. the self-selected slow speed (SS), the self-selected normal speed (SN) and the self-selected fast speed (SF). The subjects started from standing still on the treadmill for 20 seconds, and then walked with the predefined treadmill speeds. The treadmill speed changed with the sequence SN1$\Longrightarrow$SF$\Longrightarrow$SN2$\Longrightarrow$SS$\Longrightarrow$SN3, each speed lasting three minutes. Finally, the treadmill stopped and the subjects stood still for other 20 seconds. The treadmill was programmed to settle the speed changes within 1 second. After Session I, the subjects were asked to took off their sensing cuffs and then put on them again before Session II. A few minutes of rest was also allowed based on the subjects' own choice. The average SN across the subjects was 4.19 ± 0.33 km/h, and the average SS and SF were 2.88 ± 0.00 km/h and 5.02 ± 0.07 km/h, respectively.

The second experiment (Exp2) was to test the performance of the strategy in real-time gait phase estimation tasks. The experiment was conducted in Scuola Superiore Sant'Anna (Pisa, Italy). Three subjects participated in Exp2 (two males and one female), all of them provided written and informed consent. The subjects were 27.3 ± 3.2 years old. They had a height of

171 ± 3.6 cm and a weight of 67.3 ± 11.0 kg. In Exp2, the subjects wore the cuff on the left shank. A pair of insoles [26] were used to measure vertical GRF as reference of the estimated gait phase. Each insole was made of 64 optoelectronic pressure sensors which measured the pressure over the plantar area with the sampling rate of 100 Hz. The controller was implemented on the NI single board RIO (sbRIO) 9636 (National Instruments, TX, USA) to process the capacitance signals and real-time estimate the gait phase. The board was connected to capacitive sensing circuit by the serial port and to the computer by the Ethernet port. The monitor of the sensor data and the real-time supervision of the experiment were implemented with a graphical user interface (GUI). The system output the estimated gait phase in real time when the subjects walked on the treadmill. The experimental protocol of Exp2 was the same as one session of Exp1. During speed transitions, the speeds were settled within 10 seconds. In practical use, the users would change their walking speeds intuitively without the unnatural gait patterns caused by the abrupt changes of the treadmill (like Exp1). We therefore tuned the duration of speed transitions based on the experience of the subjects. The average SN across the subjects was 3.17 ± 0.15 km/h, and the average SS and SF were 2.50 ± 0.00 km/h and 4.17 ± 0.15 km/h, respectively. Before Exp2, all subjects went through the channel selection procedure to select the optimal channels (details see below). During the experiment, the capacitance signals were on-line filtered with a second-order 0.1–1 Hz band-pass Butterworth filter and were input to the estimator to estimate the gait phase.

B. Data Analysis

1) Data Segmentation Based on GRF: The collected raw capacitance signals from Exp1 were firstly filtered with a second-order band-pass Butterworth filter with the pass band 0.1–1 Hz. The band pass filter was used to remove the noises and the unnecessary variations (including noises) and keep the periodicity of the capacitance signals. The delay of the filter (within 200 ms) was negligible in the AOs based estimation method as the estimated phase was not used to match the events with physical significance. Then, in order to evaluate the signal repeatability, the signal from each channel were segmented by means of the GRF data. The foot-contact event (or heel strike event) was used to segment the data into each gait cycle. A threshold was determined to detect gait events based on initial measurements (details see [35]). After the data were collected, we calculated the gait cycle duration based on the heel strike detected by the foot pressure insole to check if there were mis-detections. If there were mis-detections, the gait cycle duration would be much smaller or larger than the others. After rechecking the data, we found out there were no mis-detections of the heel strike by the foot pressure insole.

2) Selection of the Optimal Channels: We used the segmented data to choose the optimal channels for the subsequent gait phase estimation. The selection of the optimal channels followed three criteria. Firstly, the capacitance signal should be (quasi-)periodic during walking, which means it can grasp the gait phase information. Secondly, the signal repeatability across different gait cycles should be high at different walking speeds, which insures the stability of the estimation. Thirdly, the capacitance signal should be least affected by the re-wearing of the sensing cuffs, which means the signal waveforms of the two sessions should be similar. We used the adjusted coefficients of multiple determination to evaluate the repeatability and similarity of the capacitance signals of the two experimental sessions. The adjusted coefficients of multiple determination were previously utilized to evaluate the inter-data and intra-day repeatability/similarity of the waveforms of normal gait data [37]. In order to evaluate the repeatability of the capacitance signals, for each subject, we computed the adjusted coefficient of multiple determination expressed as:

$$R_{a1}^2 = 1 - \frac{\sum_{i=1}^{M}\sum_{j=1}^{N}\sum_{t=1}^{T}(Y_{\mathrm{ijt}} - \bar{Y_{\mathrm{it}}})^2/MT(N-1)}{\sum_{i=1}^{M}\sum_{j=1}^{N}\sum_{t=1}^{T}(Y_{\mathrm{ijt}} - \bar{Y_i})^2/M(NT-1)}, \tag{9}$$

where Y_{ijt} represents the $t\text{-}th$ point of the $j\text{-}th$ gait cycle on the $i\text{-}th$ experiment session. The capacitance data of each experiment session were segmented into different gait cycles. We took the first N gait cycles to calculate R_{a1}^2, where N was the number of gait cycle of the two experiment sessions. The data of each gait cycle were interpolated to T points with the $t\text{-}th$ point representing the $t/N\%$ of one gait cycle. In Exp1, there were two experimental sessions, and the M was set to 2. As the gait cycle numbers of two experiment sessions were different, we therefore took the smaller number of the gait cycles for each subject. The average N across all the subjects were 780. The number T of interpolated points in one gait cycle was 500. $\bar{Y_{\mathrm{it}}}$ is the average value at point t on the $i\text{-}th$ experiment session, which is expressed as:

$$\bar{Y_{\mathrm{it}}} = \frac{1}{N}\sum_{j=1}^{N} Y_{\mathrm{ijt}}. \tag{10}$$

$\bar{Y_i}$ is the average value on the $i\text{-}th$ experiment session and is expressed as:

$$\bar{Y_i} = \frac{1}{NT}\sum_{j=1}^{N}\sum_{t=1}^{T} Y_{\mathrm{ijt}}. \tag{11}$$

In order to evaluate the similarity between the capacitance waveforms in Session I and Session II, we computed the adjusted coefficient of multiple determination for similarity evaluation, which is expressed as:

$$R_{a2}^2 = 1 - \frac{\sum_{i=1}^{M}\sum_{j=1}^{N}\sum_{t=1}^{T}(Y_{\mathrm{ijt}} - \bar{Y_t})^2/T(MN-1)}{\sum_{i=1}^{M}\sum_{j=1}^{N}\sum_{t=1}^{T}(Y_{\mathrm{ijt}} - \bar{Y})^2/(MNT-1)}, \tag{12}$$

where $\bar{Y_t}$ is the average of the segmented capacitance signal at point t over all the gait cycles, which is expressed as:

$$\bar{Y_t} = \frac{1}{MNT}\sum_{i=1}^{M}\sum_{j=1}^{N} Y_{\mathrm{ijt}}. \tag{13}$$

$\bar{Y}$ is the grand mean over the time and all the gait cycles which is expressed as:

$$\bar{Y} = \frac{1}{MNT}\sum_{i=1}^{M}\sum_{j=1}^{N}\sum_{t=1}^{T} Y_{\mathrm{ijt}}. \tag{14}$$

The values of R_{a1}^2 and R_{a2}^2 are between 0 and 1. If the signal waveforms show high repeatability and similarity, R_{a1}^2 and R_{a2}^2 will be close to 1, otherwise, the values will be close to 0. We calculated the adjusted coefficients of multiple determination for all the twelve subjects. For each subject, we selected two optimal signals, one measured from the thigh and one from the shank, according to the results of the indexes computation.

3) Evaluation of Gait Phase Estimation Performance: The selected channels were input in the AOs-based estimator to estimate the gait phase. In order to verify the performance of the algorithm, a benchmark phase variable $\phi_r(t)$ was built off-line within two consecutive maximum peaks of the signal selected (within the scope [0, 2π)). The estimation error was expressed as:

$$E\_Error(t,j) = \phi_r(t) - \phi(t,j), \tag{15}$$

where $E\_Error(t,j)$ was the estimation error of the $t-th$ sampling point of the $j-th$ stride; $\phi_r(t)$ was the benchmark phase of the $t-th$ sampling point; $\phi(t,j)$ was the output of the gait phase estimator. For each subject, the maximum estimation error within the stride which was defined as:

$$MAX(E\_Error) = \max_{j\in 1,\ldots,M}\sum_{t=1}^{N_j}\frac{|E\_Error(t,j)|}{N_j}, \tag{16}$$

where N_j was the number of samples within the j-th stride, and M was the number of strides to be calculated.

We calculated the root mean square value of the estimation error within the stride, which was expressed as:

$$RMS\_EWS = \frac{1}{M}\sum_{j=1}^{M}\sqrt{\frac{\sum_{t=1}^{N_j}(E\_Error(t,j))^2}{N_j}}, \tag{17}$$

where RMS_EWS was the root mean square value of the estimation error within the stride; $E\_Error(t,j)$ was the estimation error of the t-th sampling point of the j-th stride; N_j was the number of samples of the j-th stride. The number N averaged across all the subjects and all the experiment trials was 124. For each subject, the average RMS_EWS across the strides were computed to evaluate the performance. M was the number of strides to be calculated.

The gait phase reset error was also investigated. It is the difference between the estimated phase and the ideal phase (0 rad) in correspondence of the relevant gait event. In particular, we computed its root mean square value, which was expressed as:

$$RMS\_GPE = \sqrt{\frac{\sum_{j=1}^{M}(P_e(j) - P_r)^2}{M}}, \tag{18}$$

where RMS_GPE was the root mean square value of the gait phase reset error; $P_e(j)$ represented the gait phase reset error that was calculated by the estimator when the $j-th$ maximum peak of capacitance signal was detected; P_r was the ideal gait phase which was 0 rad in this study; M was the number of strides to be calculated.

In order to evaluate the performance of the gait phase estimation method with changing walking speeds. For both experiments (Exp1 and Exp2), the estimation errors, including $MAX(E\_Error)$, RMS_EWS and RMS_GPE, were calculated for all the walking speeds, all the speed transitions and all the subjects. The capacitance data and foot pressure sensor data were synchronized with the speed of treadmill. Therefore, we extracted the data of different walking speeds based on the record of the treadmill. There were four speed transitions in the experiments, including SN1→SF, SF→SN2, SN2→SS, and SS→SN3. The data of the gait cycles started from the timing point of speed changes (recorded by the treadmill) to the point that the phase error became smaller than 0.5 rad were labeled as walking speed transitions. The rest data were labeled as constant walking speeds. As the band pass filter did not converge during initial steps, we removed the data of a few steps to get useful signals. For Session I of the Exp1, the average stride number across all the twelve subjects for calculation was 627.5 $\pm$ 68.2. The number was 620.0 $\pm$ 59.0 for Session II of Exp1. For Exp2, the average stride number across all the three subjects for calculation was 577.4 $\pm$ 41.3.

An inferential non-parametric statistical test was employed in order to verify whether there were statistical differences between the two sessions in Exp1. The analysis was also carried out for Exp2 to test the statistical differences between the subjects and walking speeds.

IV. Results

A. Initial Analysis of Raw Signals

The segmented data were averaged across all the strides of a single session (see Fig. 4). As the peak-to-peak values of the raw capacitance signals were within 10 pF, we normalized the amplitude of the signals to +1 to −1 in the Fig. 4. As can be seen from Fig. 4, where the data were collected from subject 3, the signal curves of the two sessions were quantitatively similar, especially for Channel 4, Channel 5, Channel 6, Channel 7, Channel 9, Channel 11, and Channel 12. Moreover, the pre-processed capacitance signals (filtering method is described above) demonstrate quasi-sinusoidal curves across gait strides. Thus, the capacitance signals are qualified for the subsequent analysis.

B. Selection of Optimal Channels

For each subject, we selected two optimal channels, one channel was measured from the thigh cuff and the other from the shank. The values of R_{a1}^2 and R_{a2}^2 were shown in the Tables I and II, respectively. In the tables, CHx, $x = 1, 2, ..., 12$, represent channel x. Sx, $x = 1, 2, ..., 12$ represent subject x. The values that were closer to 1 indicated better performance (higher signal repeatability and similarity). The words in boldface indicated the selected optimal channels.

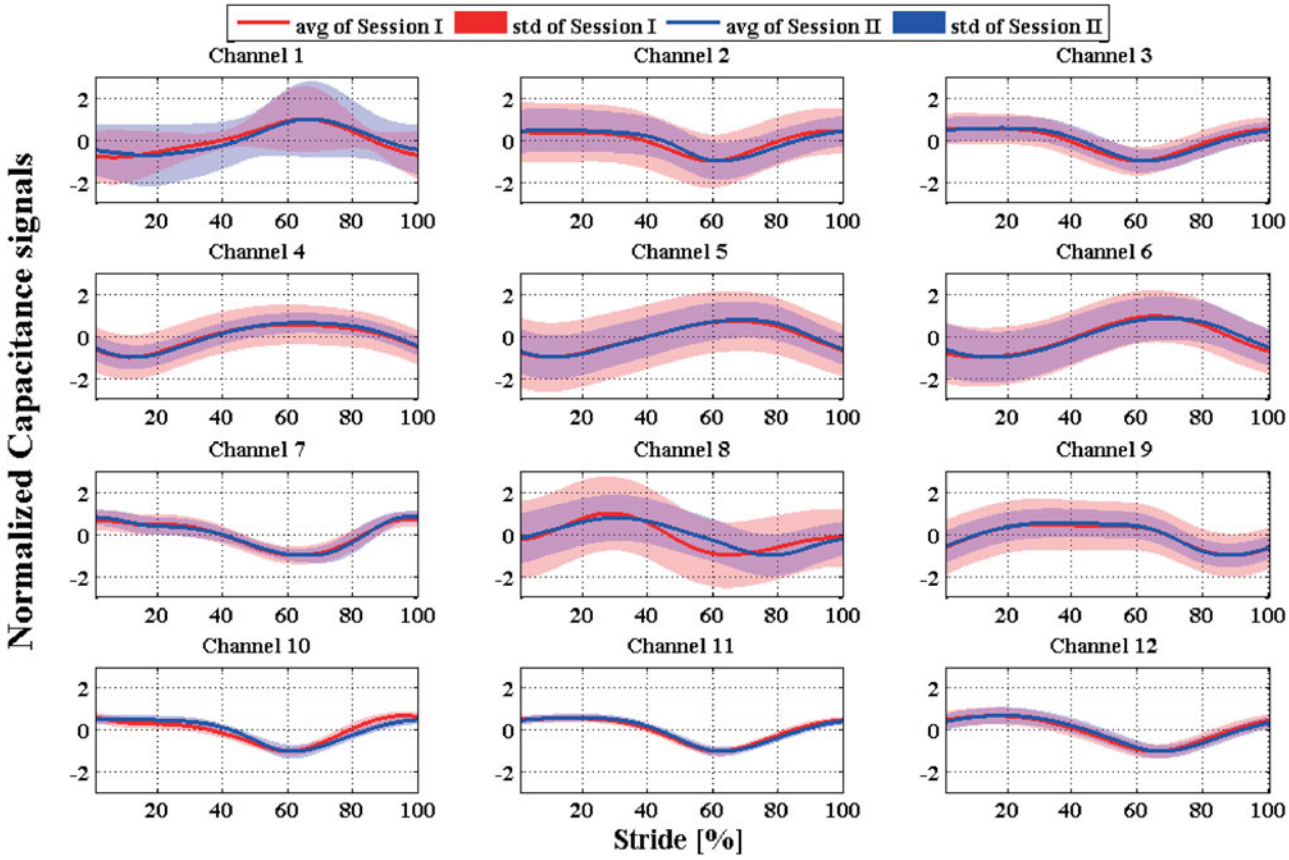

Fig. 4. The normalized capacitance signals in one stride of Exp 1. The horizontal axis represents the percentage of one gait cycle from 0% to 100%. The vertical axis represents the normalized signals. The 12 subfigures show the twelve channels of capacitance signals. Channels 1–6 are electrodes on the sensing cuff of the thigh while the remaining channels are located on the shank. In each subfigure, the red line and the blue line represent the normalized signals of the Session I and the Session II, respectively. The shaded ares represent the standard deviation of the signals. The normalized signals were averaged across all the strides in Exp1 and time normalized to one stride. Data were collected from subject 3 in Exp1. The gait strides were segmented by the GRF signal of the pressure insole.

TABLE I
THE VALUES OF R_{a1}^2 WHICH REPRESENT SIGNAL REPEATABILITY FOR ALL THE SIGNAL CHANNELS AND ALL THE SUBJECTS

Subject number	channel number 1–12											
	CH1	CH2	CH3	CH4	CH5	CH6	CH7	CH8	CH9	CH10	CH11	CH12
S1	0.450	0.636	0.000	0.933	**0.948**	0.887	0.515	0.236	0.688	0.673	**0.864**	0.544
S2	0.164	0.803	0.031	**0.966**	0.951	0.966	0.812	0.953	0.888	0.946	0.966	**0.938**
S3	0.874	0.919	0.000	0.946	0.966	**0.961**	0.895	0.860	0.932	0.938	**0.967**	0.964
S4	0.869	0.914	0.011	0.905	0.960	**0.962**	0.815	0.845	0.916	0.912	**0.962**	0.852
S5	0.299	0.940	0.078	0.762	0.969	**0.960**	0.934	0.931	0.063	0.935	**0.938**	0.918
S6	0.914	0.877	0.449	0.940	0.944	**0.950**	0.919	0.895	0.107	0.883	0.832	**0.900**
S7	0.949	0.917	0.076	0.418	0.934	**0.933**	0.939	0.915	0.077	**0.957**	0.961	0.968
S8	0.981	0.825	0.094	0.848	0.964	**0.968**	0.926	0.946	0.091	**0.965**	0.965	0.946
S9	0.936	0.859	0.942	0.949	0.966	**0.977**	0.587	0.634	0.000	**0.835**	0.635	0.874
S10	0.937	0.707	0.012	0.875	**0.967**	0.966	0.821	0.892	0.018	0.943	**0.958**	0.941
S11	0.896	0.514	0.934	0.930	0.948	**0.956**	0.820	**0.872**	0.062	0.687	0.582	0.560
S12	0.481	0.784	0.962	0.919	0.978	**0.982**	0.775	0.452	0.241	0.652	**0.902**	0.933

As it was seen from the tables, although individual differences existed, there were some similar trends for the two indexes. First of all, for signal repeatability and similarity, the channels on the posterior part of the leg showed better performance than that on the anterior side. Except S11, the optimal channels for all the other subjects were on the posterior leg ($CH4$, $CH5$, $CH6$ for the thigh, and $CH10$, $CH11$, and $CH12$ for the shank). Second, among all the signal channels, $CH5$, $CH6$, $CH10$ and $CH11$ performed better than the other channels. The values of R_{a1}^2 and R_{a2}^2 were closer to 1 than the other

TABLE II
THE VALUES OF R^2_{a2} WHICH REPRESENT SIMILARITY OF SIGNAL WAVEFORMS FOR ALL THE SIGNAL CHANNELS AND ALL THE SUBJECTS

Subject number	channel number 1–12											
	CH1	CH2	CH3	CH4	CH5	CH6	CH7	CH8	CH9	CH10	CH11	CH12
S1	0.187	0.441	0.000	0.910	**0.947**	0.864	0.348	0.233	0.650	0.666	**0.854**	0.501
S2	0.050	0.802	0.037	**0.949**	0.889	0.816	0.789	0.919	0.864	0.886	0.778	**0.914**
S3	0.813	0.891	0.011	0.896	0.942	**0.957**	0.853	0.801	0.869	0.896	**0.960**	0.957
S4	0.808	0.886	0.007	0.891	0.937	**0.954**	0.743	0.812	0.847	0.889	**0.955**	0.952
S5	0.283	0.698	0.046	0.656	0.824	**0.890**	0.701	0.890	0.064	0.782	**0.805**	0.849
S6	0.896	0.678	0.221	0.864	0.934	**0.946**	0.833	0.842	0.000	0.867	0.825	**0.886**
S7	0.850	0.871	0.060	0.274	0.848	**0.865**	0.739	0.793	0.066	**0.928**	0.836	0.916
S8	0.980	0.657	0.105	0.709	0.963	**0.967**	0.874	0.843	0.058	**0.740**	0.966	0.887
S9	0.892	0.729	0.859	0.833	0.926	**0.950**	0.148	0.435	0.000	**0.821**	0.591	0.745
S10	0.873	0.488	0.024	0.772	**0.886**	0.755	0.669	0.857	0.029	0.839	**0.929**	0.915
S11	0.856	0.288	0.838	0.874	0.880	**0.922**	0.672	**0.741**	0.063	0.507	0.539	0.488
S12	0.352	0.453	0.812	0.864	0.937	**0.915**	0.546	0.288	0.198	0.608	**0.881**	0.911

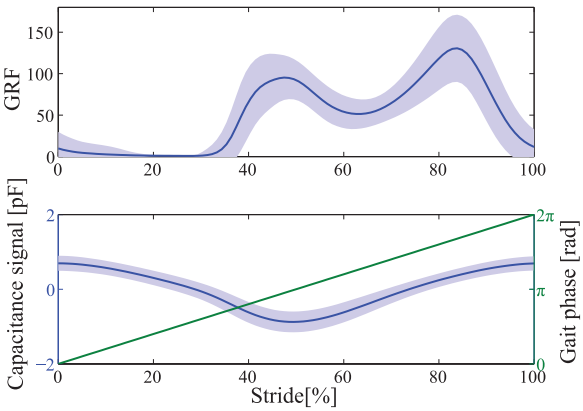

Fig. 5. The segmented data by the maximum peak of capacitance signals. The horizontal axis represents the percentage of a stride from 0% to 100%. The left vertical axis denotes the vertical ground reaction force (GRF) signal (top) and the capacitance signal (bottom). The normalized GRF signals are proportional to actual force. The right vertical axis represents the benchmark gait phase variable. The two subfigures show the GRF signal (top) and the capacitance signal (bottom) that are normalized to one gait stride. The stride is segmented by the maximum peak of the capacitance signal. The average values of signals across different strides and their standard deviations are shown as the blue line and the shaded area, respectively. The green line denotes the benchmark gait phase variable changing from 0 to 2π rad in one stride.

channels. The optimal channels (as highlighted in boldface in Tables I and II) were selected by taking the two indexes and the periodicity of the signals into consideration. After selection of the optimal channels, the selected capacitance signal was input to the AOs dynamical system and to the subsequent blocks (Fig. 1). In this study, the gait phase was reset in correspondence of the maximum peak of the selected capacitance signals. The segmented signal by the capacitance signal was shown in Fig. 5. The case data were collected from $CH6$ of subject 11.

C. Offline Gait Phase Estimation

The average stride numbers of speed transitions were shown as Table III. The gait phase estimation strategy produced low estimation errors in Exp1, either for different constant walking speeds (see Fig. 6) or during walking speed transitions (see Fig. 7). For the results of constant walking speeds, there were no extremely large estimation errors among all the speeds (Fig. 6). The average $MAX(E\_Error)$ values for constant speed were 0.17 rad for the thigh and 0.30 rad for the shank. They accounted for 2.7% and 4.9% of one gait cycle. The average RMS_EWS were 0.19 rad (0.30%) for the thigh and 0.35 rad (5.6%) for the shank. The average RMS_GPE for constant walking speeds were 0.24 rad (3.6%) and 0.40 rad (6.4%) for the thigh and the shank, respectively. Compared with constant speeds, the estimation errors during speed transitions were a little higher (approximately 0.1 rad difference in average, see Fig. 7). The average $MAX(E\_Error)$ values during speed transitions were 0.34 rad (5.4%) for the thigh and 0.42 rad (6.7%) for the shank. The average RMS_EWS were 0.31 rad (4.9%) for the thigh and 0.43 rad (6.8%) for the shank. The average RMS_GPE for constant walking speeds were 0.33 rad (5.3%) and 0.45 rad (7.2%) for the thigh and the shank, respectively. We also investigated the maximum gait phase reset errors in the trials. The average values of the maximum gait phase reset errors across all the subjects were 1.07 rad (thigh cuff in Session I), 1.25 rad (thigh cuff in Session II of Exp1), 1.40 rad (shank cuff in Session I of Exp1) and 1.52 rad (shank cuff in Session II of Exp1). In addition, the maximum values of $|E\_Error(t, j)|$ in the trial and the corresponding stride numbers after speed changes were calculated. The average values across the subjects were 0.60 ± 0.39 rad, 0.42 ± 0.21 rad, 0.78 ± 0.26 rad and 0.81 ± 0.30 rad

TABLE III
THE STRIDE NUMBERS OF THE SPEED TRANSITIONS OF EXP1 FOR ALL THE SUBJECTS

Position/Session	Speed transition			
	SN1→SF	SF→SN2	SN2→SS	SS→SN3
Thigh/I	11.8 ± 4.8	13.3 ± 6.7	11.8 ± 6.0	13.1 ± 4.7
Thigh/II	10.5 ± 6.3	13.5 ± 9.0	10.1 ± 4.4	12.1 ± 5.9
Shank/I	10.7 ± 4.5	12.6 ± 6.6	12.2 ± 3.7	13.2 ± 6.6
Shank/II	15.0 ± 5.8	12.0 ± 4.2	11.8 ± 5.5	14.3 ± 6.1

The values are Mean±STD.

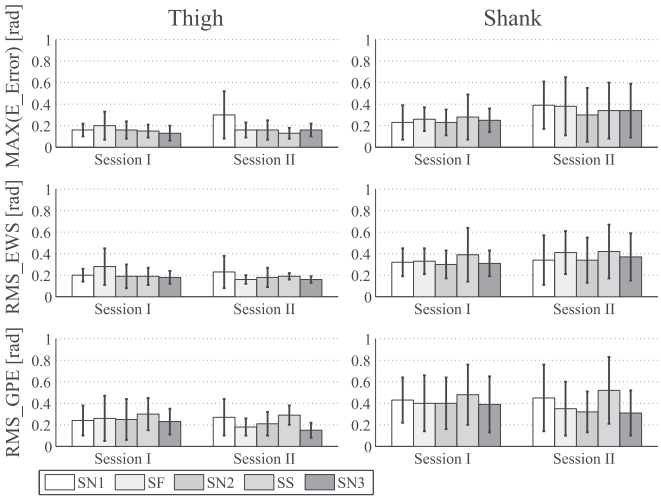

Fig. 6. The gait phase estimation results of constant speeds of Exp1. The three rows of subfigures show the results of $MAX(E\_Error)$ (rop row), RMS_EWS (the middle row) and RMS_GPE (bottom row). The left column of the subfigures are the results produced by the channel on the thigh, while the right one show that on the shank. The average values of the estimation errors of different walking speeds are shown in different gray-scale. In the figures, SN represents the normal walking speed; SF represents the fast walking speed; and SS represents the slow walking speed. Data were collected from the twelve subjects of Exp1. The error bars represent AVE±STD across all the subjects.

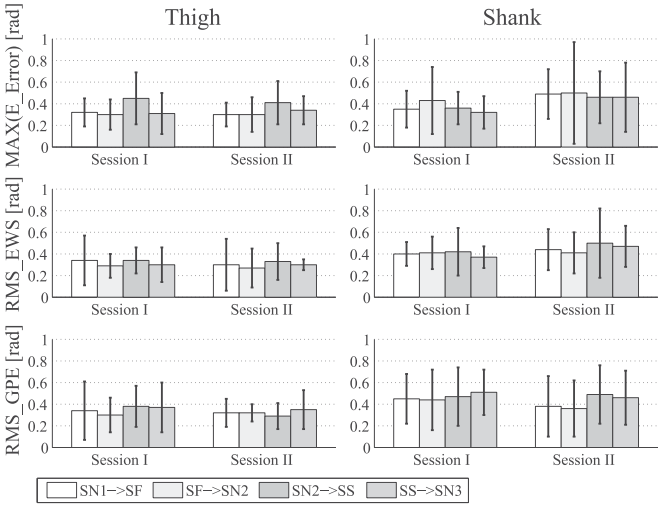

Fig. 7. The gait phase estimation results during the speed transitions of Exp1. The three rows of subfigures show the results of $MAX(E\_Error)$ (rop row), RMS_EWS (the middle row) and RMS_GPE (bottom row). The left column of the subfigures are the results produced by the channel on the thigh, while the right one show that on the shank. The average values of the estimation errors of different speed transitions are shown in different gray-scale. Data were collected from the twelve subjects of Exp1. The error bars represent AVE±STD across all the subjects.

for thigh cuff in session I, thigh cuff in Session II, shank cuff in Session I and shank cuff in Session II, respectively. The corresponding stride numbers (averaged across the subjects) were 2.08 ± 1.06, 4.00 ± 2.70, 5.50 ± 2.02 and 3.92 ± 2.02. Among all the subjects, the maximum error (1.65 rad) occurred at the second stride during SN1→SF in Session I of S1, when the data of the thigh cuff were used.

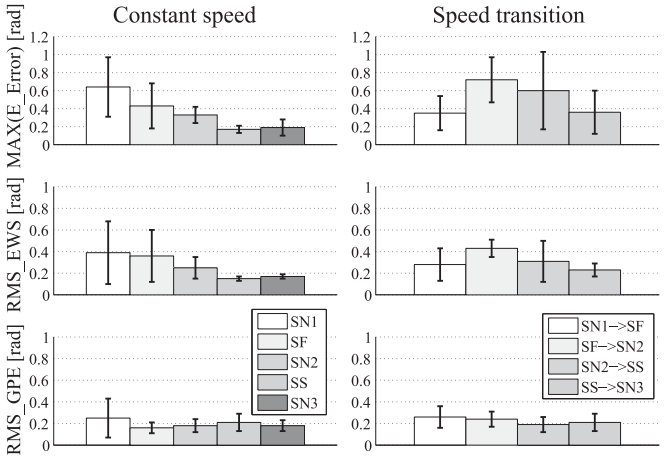

Fig. 8. The gait phase estimation results of Exp2. The three rows of subfigures show the results of $MAX(E\_Error)$ (rop row), RMS_EWS (the middle row) and RMS_GPE (bottom row). The left column of the subfigures are the results of constant walking speeds, while the right one show the results during speed transitions. The average values of the estimation errors of different walking speeds and speed transitions are shown in different gray-scale, as is denoted by the legends. In the figures, SN represents the normal walking speed; SF represents the fast walking speed; and SS represents the slow walking speed. Data were collected from the three subjects of Exp2. Data were collected from three subjects of Exp2. The error bars represent ±STD across all the subjects.

Statistical tests were also carried out to evaluate the difference of the estimation errors between the two experiment sessions, both for the constant speeds and speed transitions. As the data were not normally distributed according to the Kolmogorov-Sminorv test, we conducted Wilcoxon signed rank test with the significance level of 5%. All the p values were larger than 0.05. There was no statistical evidence that re-wearing the cuffs affected the estimation accuracies, both for the constant speed conditions and with speed transitions. Friedman test (significance level 1%) was conducted to evaluate the statistical difference between different walking speeds and subjects. There was not statistical evidence that the subjects and walking speeds affected the algorithm performance, both for constant speed conditions and the speed transitions ($p > 0.01$, Friedman test). One exception was RMS_GPE for the thigh cuff during the speed transitions in Session II of Exp1 ($p = 0.003$, Friedman test).

D. Real-Time Gait Phase Estimation

The gait phase estimation strategy was able to estimate the gait phase with similar performances for all the subjects on different walking speeds (see Fig. 8). As it has been proved by the off-line estimation performance, both sensing cuffs could produce an accurate estimation independently. Therefore, in Exp2, we only used the sensing cuff on the shank. In order to make the system more robust, two different capacitance signals were selected. Signal from channel 10 was used to learn the phase and signal from channel 11 was used to detect the gait event (maximum peak). The average values of constant speeds were 0.35 rad (5.6%), 0.26 rad (4.1%) and 0.20 rad (3.2%) for $MAX(E\_Error)$, RMS_EWS and RMS_GPE,

respectively. The average stride numbers of the speed transitions were 14.0, 13.7, 14.7 and 12.7 for SN1→SF, SF→SN2, SN2→SS and SS→SN3, respectively. The average values during speed transitions were 0.51 rad (8.1%), 0.31 rad (4.9%) and 0.23 rad (3.6%) for $MAX(E\_Error)$, RMS_EWS and RMS_GPE, respectively. For the real-time gait phase estimation, the RMS_EWS and RMS_GPE were in the same level between the constant speeds and speed transitions. For the $MAX(E\_Error)$, the average values of speed transitions were 0.15 rad higher than that of constant speeds. For the on-line estimation, the largest phase reset errors were 1.26 rad (occurred in SN1) for S1, 0.74 rad (occurred in SN1) for S2 and 0.91 rad (occurred in SS) for S3. The largest estimation errors within the stride were 0.95 rad (4th stride of SN1→SF) for S1, 0.98 rad (3rd stride of SF→SN2) for S2, and 0.69 rad (1st stride of SF→SN2) for S3. Friedman test (significance level 1%) was also conducted for the real-time estimation. There was not statistical evidence that the subjects and walking speeds affected the algorithm performance, both for constant speed conditions and the speed transitions ($p > 0.01$, Friedman test). More information of real-time estimation can be found in the video attached.

V. Discussion

In this study, we validated the effectiveness of the strategy for gait phase estimation. The noncontact system achieved accurate and continuous gait phase estimation without fixing electrodes on the skin. The capacitance signals measured from the posterior side of the leg showed high repeatability across different strides and small inter-subject variability on various walking speeds. With the selected optimal channels, the strategy produced fairly low error rates on multiple subjects. The system was also found to be robust when it went through the disturbance of re-wearing the sensing cuffs. Moreover, the real-time gait phase estimation performance was comparable with the off-line results. Our approach is a promising alternative to the IMU based, foot pressure based and sEMG based strategies for exoskeleton/orthosis control.

Our strategy has three advantages over the existing strategies. Firstly, compared with the foot pressure sensors which are subjected to the overloads, our sensing system measures signals from the leg, in which the electrodes bear much smaller pressure than foot pressure sensors. The failure of the system caused by repeated load will not be a problem for our sensing strategy. Consequently, the lifespan and reliability of the system will be increased. Secondly, compared with IMUs, the capacitive sensing system can be fabricated either with hard materials on cuffs of the exoskeletons or with soft materials on clothes. The system is less obtrusive and can be more stable than the rigid nodes of IMUs on human body. Thirdly, our strategy demonstrated to be effective and robust after the sensory system was re-worn. It overcame the drawbacks of the sEMG systems which need to directly contact the skin and are easily affected by the sensing positions. In clinical use, our system will be conveniently and comfortably worn without the help of experienced clinical personnel, increasing the usability of the whole apparatus.

Compared with existing studies that achieved continuous gait phase estimation by other sensing approaches [29]–[31], our strategy produced comparable accuracies. In the study of [29], the researchers estimated the gait phase by the prediction to the duration of the current stride. The accuracy is negatively affected by walking speed changes [31]. By comparison, in our study, the capacitance signals can be tracked by the AOs-based estimator when walking speed changes. There is no significant difference of the accuracies among the different walking speeds ($p > 0.01$, Friedman test). The researchers of [31] designed AOs estimation method based on inertial signals (hip joint angles measured by absolute encoders) and foot pressure signals (GRF measured by foot insole). The study achieved the highest accuracies among the studies that involved continuous gait phase estimation. The maximum phase errors within the strides were 0.09 rad by using hip joint angles and 0.12 rad by using GRF [31]; the maximum root mean squares of the gait phase errors were 0.07 by using hip joint angles and 0.16 rad by using GRF. For the off-line results in our study, the channels on the thigh cuff produced lower errors that on the shank. The maximum average $MAX(E_Error)$s were 0.30 rad (SN1 of Session I, see Fig. 6) for constant walking speeds and 0.45 rad (SN2→SS of Session I, see Fig. 7) for speed transitions. The results were obtained with the capacitance signals which compensated the limitations of the GRF and the inertial signals used by [31] (as mentioned in the above paragraph). Although the errors were a little higher than that in [31], the estimation results in our study was achieved with re-wearing the sensing cuffs in the middle, the task of which was more complicated. The stability of the system against re-wearing the sensing devices is crucial for the real application of the exoskeletons. We therefore tuned the parameters of the estimator by trading off between the estimation accuracies and the model fitting (to avoid over fitting).

In this study, the selected optimal channels concentrated on the dorsal side of the leg. There are two explanations. Firstly, the capacitance signals reflect the muscle volume changes during ambulation. For the shank, the muscles on the posterior leg (such as Gastrocnemius muscle) have larger volume than that on the anterior leg (tibialis anterior), and thus show more prominent changes in capacitance signals. Secondly, for the thigh, although the muscle volume is similar for the two sides of leg, the shape changes caused by the muscle contractions on the dorsal side of the thigh have smaller variability than that of the frontal side. Therefore, the capacitance signals on this side are more stable and repeatable across gait cycles. The inter-subject and intra-subject similarity would be beneficial for future implementation of the system on exoskeletons and orthoses. There is no necessity to re-configure the system if the subject changes or re-wears the device. We also compared the capacitance signals with the gait cycle segmented by heel-strike of the GRF signal. The percentage of the gait cycle at maximum/minimum peaks of the capacitance signals were calculated. Although individual difference exists, there are some channels (channel 5, 6 and 11) that show similar trends across the subjects at the peaks of the signals. The maximum peak was 67.08 ± 3.96% of the stride (started from the heel-strike detected by GRF) for the signal measured from channel 5, 65.58 ± 4.32% of the stride for the

signal measured from channel 6 and 23.09 $\pm$ 4.95% of the stride for signal measured from channel 11. The minimum peak was 14.33 $\pm$ 4.90% of the stride for the signal measured from channel 5, 15.17 $\pm$ 5.61% of the stride for the signal measured from channel 6 and 67.30 $\pm$ 6.07% of the gait cycle for signal measured from channel 11.

In Exp2, only the sensing cuff on the shank was used, while in Exp1, the sensing cuff on the thigh produced higher estimation accuracy than that of the shank. In this study, we took not only the estimation accuracy into consideration, but the wearing stability as well. In terms of wearing stability, the cuff on the shank was more stable than that of the thigh. For the cuff on the shank, the prominent part of the gastrocnemius muscle on the posterior side of the leg can prevent the cuff from gliding down. As the thigh shows the shape of an inverted cone, there is no such position on the thigh that can prevent the cuff from gliding down. Exp2 was the real-time gait phase estimation of which the condition was closer to practical applications but was more complicated. To make the performance stable, we chose the shank cuff for Exp2. In future study, we plan to apply the sensing approach on exoskeletons. The sensing device can be integrated on the mechanical structure of the exoskeleton. The problem of sliding down of the sensing cuff on the thigh will be addressed.

Although the gait phase estimation results are encouraging in this study, limitations still exist. Firstly, the system was validated only on healthy subjects in treadmill walking trials. The evaluation of the feasibility of gait phase estimation on patients with gait disorders in an unstructured environment such as free ground-level walking, stairs/ramps walking have not been investigated. The performance of the system with exoskeletons and orthoses has not been evaluated. Secondly, it took about 10 steps in average for the estimator to converge again (phase error returned below 0.5 rad) in speed transitions. During the speed transitions, the subjects had to adjust their postures to get used to the new walking speeds for a few steps. The change of the signal waveform resulted in the increase of the $F(t)$. The estimator therefore needed a period of time (depends on the learning rate) to synchronize with the new waveform. Thirdly, although the strategy can perform accurate estimation with only one channel of capacitance signal, the optimal channel selection procedure was needed for each subject before the actual estimation, which increased the complexity of the system. Future works will be focused on the following aspects to address the limitations. First of all, experiments on subjects with gait disorders will be carried out to evaluate the proposed strategy. In addition to the task of level walking, other locomotion modes such as stair ascending/descending, ramp ascending/descending and free ground-level walking will be studied. Extensive experiments of on-line control of the exoskeletons based on the gait phase estimation strategy will be conducted. Secondly, the gait phase estimation method will be improved by combining different signal channels to remove the procedure of channel selection and by developing dynamical learning algorithm to further increase the estimation performance (accuracy and adapting time) in speed transition period. The customized cuffs and sensing front-ends will be developed to make it more adaptive to different users. Thirdly, development of capacitive sensing system with soft materials and customized sizes will be carried out, to make it compatible with soft assitive wearable robots.

VI. Conclusion

In this study, we designed a gait phase estimation strategy which was composed of a noncontact capacitive sensing system and an AOs based gait phase estimator. We validated the strategy through level walking experiments with various walking speeds and re-wearing the sensing device. We also proved that the system achieved equally well performance in the real-time estimation. This study provided a promising alternative solution to continuous gait phase estimation for exoskeleton/orthosis control. Future efforts will be made to on-line control of exoskeletons/orthoses in practical use.

References

[1] A. M. Dollar and H. Herr, "Lower extremity exoskeletons and active orthoses: Challenges and state-of-the-art," *IEEE Trans. Robot.*, vol. 24, no. 1, pp. 144–158, Feb. 2008.

[2] T. Yan *et al.*, "Review of assistive strategies in powered lower-limb orthoses and exoskeletons," *Robot. Auton. Syst.*, vol. 64, pp. 120–136, 2015.

[3] A. Esquenazi, "The rewalk powered exoskeleton to restore ambulatory function to individuals with thoracic-level motor-complete spinal cord injury," *Amer. J. Phys. Med. Rehabil.*, vol. 91, no. 11, pp. 911–921, 2012.

[4] D. Sanz-Merodio *et al.*, "Generation and control of adaptive gaits in lower-limb exoskeletons for motion assistance," *Adv. Robot.*, vol. 28, no. 5, pp. 329–338, 2014.

[5] H. Kazerooni *et al.*, "On the control of the berkeley lower extremity exoskeleton (BLEEX)," in *Proc. IEEE Int. Conf. Robot. Autom.*, 2005, pp. 4353–4360.

[6] Y. Sankai, "HAL: Hybrid assistive limb based on cybernics," *Robot. Res.*, vol. 66, pp. 25–34, 2011.

[7] K. Kong and D. Jeon, "Design and control of an exoskeleton for the elderly and patients," *IEEE/ASME Trans. Mechatronics*, vol. 11, no. 4, pp. 428–432, Aug. 2006.

[8] K. Shamaei *et al.*, "Design and evaluation of a quasipassive knee exoskeleton for investigation of motor adaptation in lower extremity joints," *IEEE Trans. Biomed. Eng.*, vol. 61, no. 6, pp. 1809–1821, Jun. 2014.

[9] A. T. Asbeck *et al.*, "Stronger, smarter, softer next-generation wearable robots," *IEEE Robot. Autom. Mag.*, vol. 21, no. 4, pp. 22–33, Dec. 2014.

[10] G. Colombo *et al.*, "Treadmill training of paraplegic patients using a robotic orthosis," *J. Rehabil. Res. Develop.*, vol. 37, no. 6, pp. 693–700, 2000.

[11] J. F. Veneman *et al.*, "Design and evaluation of the LOPES exoskeleton robot for interactive gait rehabilitation," *IEEE Trans. Neural Syst. Rehabil. Eng.*, vol. 15, no. 3, pp. 379–386, Sep. 2007.

[12] V. Bartenbach *et al.*, "Concept of a soft exosuit for the support of leg function in rehabilitation," in *Proc. IEEE Int. Conf. Rehabil. Robot.*, 2015, pp. 125–130.

[13] J. Bae *et al.*, "A soft exosuit for patients with stroke: Feasibility study with a mobile off-board actuation unit," in *Proc. IEEE Int. Conf. Rehabil. Robot.*, 2015, pp. 131–138.

[14] R. Ronsse *et al.*, "Oscillator-based assistance of cyclical movements: Model-based and model-free approaches," *Med. Biol. Eng. Comput.*, vol. 49, no. 10, pp. 1173–1185, 2011.

[15] F. Giovacchini *et al.*, "A light-weight active orthosis for hip movement assistance," *Robot. Auton. Syst.*, vol. 73, pp. 123–134, 2013.

[16] M. R. Tucker *et al.*, "Control strategies for active lower extremity prosthetics and orthotics: A review," *J. NeuroEng. Rehabil.*, vol. 12, no. 1, p. 1, 2015.

[17] J. Taborri *et al.*, "Gait partitioning methods: A systematic review," *Sensors*, vol. 16, no. 1, pp. 66–85, 2016.

[18] J. Y. Jung *et al.*, "A neural network-based gait phase classification method using sensors equipped on lower limb exoskeleton robots," *Sensors*, vol. 15, no. 11, pp. 27738–27759, 2015.

[19] D. Kotiadis *et al.*, "Inertial gait phase detection for control of a drop foot stimulator: Inertial sensing for gait phase detection," *Med. Eng. Phys.*, vol. 32, no. 4, pp. 287–297, 2010.

[20] M. S. H. Aung *et al.*, "Automated detection of instantaneous gait events using time frequency analysis and manifold embedding," *IEEE Trans. Neural Syst. Rehabil. Eng.*, vol. 21, no. 6, pp. 908–916, Nov. 2013.
[21] A. Mannini *et al.*, "Online decoding of hidden Markov models for gait event detection using foot-mounted gyroscopes," *IEEE J. Biomed. Health Informat.*, vol. 18, no. 4, pp. 1122–1130, Jul. 2014.
[22] L. M. Mooney *et al.*, "Autonomous exoskeleton reduces metabolic cost of human walking during load carriage," *J. NeuroEng. Rehabil.*, vol. 11, 2014, Art. no. 80.
[23] A. T. Asbeck *et al.*, "Multi-joint soft exosuit for gait assistance," in *Proc. IEEE Int. Conf. Robot. Autom.*, 2015, pp. 6197–6204.
[24] I. P. I. Pappas *et al.*, "A reliable gait phase detection system," *IEEE Trans. Neural Syst. Rehabil. Eng.*, vol. 9, no. 2, pp. 113–125, Jun. 2001.
[25] K. Kyoungchul and M. Tomizuka, "A gait monitoring system based on air pressure sensors embedded in a shoe," *IEEE/ASME Trans. Mechatronics*, vol. 14, no. 3, pp. 358–370, Jun. 2009.
[26] S. Crea *et al.*, "A wireless flexible sensorized insole for gait analysis," *Sensors*, vol. 14, no. 1, pp. 1073–1093, 2014.
[27] M. Meng *et al.*, "EMG signals based gait phases recognition using hidden Markov models," in *Proc. Int. Conf. Inf. Autom.*, 2010, pp. 852–856.
[28] C. D. Joshi *et al.*, "Classification of gait phasesfrom lower limb EMG: Application to exoskeleton orthosis," in *Proc. IEEE-EMBS Special Topic Conf. Point-of-Care Healthc. Technol.*, 2013, pp. 228–231.
[29] C. L. Lewis and D. P. Ferris, "Invariant hip moment pattern while walking with a robotic hip exoskeleton," *J. Biomech.*, vol. 44, no. 5, pp. 789–793, 2011.
[30] T. Lenzi *et al.*, "Powered hip exoskeletons can reduce the user's hip and ankle muscle activations during walking," *IEEE Trans. Neural Syst. Rehabil. Eng.*, vol. 21, no. 6, pp. 938–948, Nov. 2013.
[31] T. Yan *et al.*, "An oscillator-based smooth real-time estimate of gait phase for wearable robotics," *Auton. Robot.*, vol. 41, pp. 759–774, 2017.
[32] Y. Menguc *et al.*, "Soft wearable motion sensing suit for lower limb biomechanics measurements," in *Proc. IEEE Int. Conf. Robot. Autom.*, 2013, pp. 5309–5316.
[33] A. H. A. Razak *et al.*, "Foot plantar pressure measurement system: A review," *Sensors*, vol. 12, no. 7, pp. 9884–9912, 2012.
[34] E. Zheng *et al.*, "A noncontact capacitive sensing system for recognizing locomotion modes of transtibial amputees," *IEEE Trans. Biomed. Eng.*, vol. 61, no. 12, pp. 2911–2920, Dec. 2014.
[35] E. Zheng and Q. Wang, "Noncontact capacitive sensing-based locomotion transition recognition for amputees with robotic transtibial prostheses," *IEEE Trans. Neural Syst. Rehabil. Eng.*, vol. 25, no. 2, pp. 161–170, 2017.
[36] R. Ronsse *et al.*, "Real-time estimate of velocity and acceleration of quasiperiodic signals using adaptive oscillators," *IEEE Trans. Robot.*, vol. 29, no. 3, pp. 783–791, Jun. 2013.
[37] M. P. Kadaba *et al.*, "Repeatability of kinematic, kinetic, and electromyographic data in normal adult gait," *J. Orthopaedic Res.*, vol. 7, no. 6, pp. 849–860, 1989.

Enhao Zheng received the bachelor's degree in automatic control from Xidian University, Xi'an, China, in 2010, and the Ph.D. degree in dynamics and control from Peking University, Beijing, China, in 2016. He is currently an Assistant Professor with the State Key Laboratory of Management and Control for Complex Systems, Institute of Automation, Chinese Academy of Sciences, Beijing, China. His research interests include human motion detection, capacitive sensing, and human–machine interface.

Silvia Manca received the B.Sc. and M.Sc. degree in biomedical engineering from the University of Pisa, Pisa, Italy, in 2012 and 2015 respectively. She joined The BioRobotics Institute, Scuola Superiore Sant'Anna, Pontedera, Italy, in 2014, as a master thesis student. She is currently a Postgraduate Researcher with the Wearable Robotics laboratory, Scuola Superiore Sant'Anna. Her research interests include the development and validation of adaptive strategies and investigation of novel cognitive interfaces for the control of lower-limb wearable robots.

Tingfang Yan received the M.Sc. degree in control science and engineering from Shandong University, Jinan, China, in 2014, and the Ph.D. degree (*cum laude*) from the BioRobotics Institute, Scuola Superiore Sant'Anna, Pisa, Italy, in 2016. She is currently a Research Associate with the Department of Electronic Engineering, The Chinese University of Hong Kong, Hong Kong. She participated in the European research project CYBERLEGs with major roles in the design and validation of assistive strategies for powered lower limb orthoses. Her main research interests include the development of wearable robotic devices for human motion assistance and rehabilitation.

Andrea Parri received the M.Sc. degree in biomedical engineering (*cum laude*) from the University of Pisa, Pisa, Italy, in April 2014. He is currently working toward the Ph.D. degree in biorobotics with the Wearable Robotics Laboratory, The BioRobotics Institue, Scuola Superiore Sant'Anna, since November 2014. His major research interests include the design, development, and validation of adaptive control architectures for lower-limb wearable robots.

Nicola Vitiello received the M.Sc. degree in biomedical engineering from the University of Pisa, Pisa, Italy, in 2006, and from Scuola Superiore Sant'Anna (SSSA), Pisa, in 2007. He then received the Ph.D. degree in biorobotics from SSSA in 2010. He is currently an Associate Professor with The BioRobotics Institute, SSSA, where he leads the Wearable Robotics Laboratory. He has authored or coauthored 50 ISI/Scopus papers, more than 30 peer-reviewed conference proceedings papers, and ten patent applications. He has served as the Scientific Secretary of the EU FP7 CA-RoboCom project, and he was the scientific project coordinator of the EU FP7 CYBERLEGs project, the EARLYREHAB project funded by Regione Toscana, and the IUVO research project funded by a local bank Foundation, namely "Fondazione Pisa." He is currently the Scientific Project Coordinator of the H2020-ICT-CYBERLEGs Plus Plus project, and partner of the H2020-ICT-AIDE and H2020-FoF-HUMAN projects. He is a co-founder and shareholder of the spin-off company IUVO S.r.l. His research interests include the development, experimental validation, and maturation of novel wearable robotic devices for human movement assistance, rehabilitation, and augmentation.

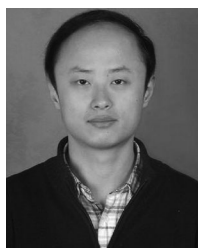

Qining Wang (S'06–M'09) received the bachelor's degree in computer science and technology from China University of Geosciences, Beijing, China, in 2004, and the Ph.D. degree in dynamics and control from Peking University, Beijing, in 2009. He was an Assistant Professor with the Center for Systems and Control, College of Engineering, Peking University, from July 2009 to July 2012. He is currently a Tenured Associate Professor with the College of Engineering, Peking University, and the Director of the Beijing Engineering Research Center of Intelligent Rehabilitation Engineering. He is the Project Leader of the Robotic Prosthesis R&D Group, Peking University. He has authored/coauthored more than 120 scientific papers in international journals and refereed conference proceedings. His research interests include bioinspired robots and rehabilitation robotics. He (with his colleagues) received the Best Technical Paper Award at the 17th International Conference on Climbing and Walking Robots and the 18th International Conference on Climbing and Walking Robots. He serves as the Associate Editor of the IEEE ROBOTICS AND AUTOMATION MAGAZINE.